2003

Size Selective Recognition of siRNA by an RNA Silencing Suppressor

Jeff Vargason
George Fox University, jvargason@georgefox.edu

Gyorgy Szittya
Plant Biology Institute, Godollo, Hungary

Jozsef Burgyan
Plant Biology Institute, Godollo, Hungary

Traci M. Tanaka Hall
National Institute of Environmental Health Sciences, North Carolina

Recommended Citation
Previously published in Cell, December 2003, vol. 115, pp. 799–811 http://www.sciencedirect.com/science/article/pii/S009286740300984X

Size Selective Recognition of siRNA by an RNA Silencing Suppressor

Jeffrey M. Vargason,[1] György Szittya,[2] József Burgyán,[2] and Traci M. Tanaka Hall[1,*]
[1]Laboratory of Structural Biology
National Institute of Environmental Health Sciences
National Institutes of Health
Research Triangle Park, North Carolina 27709
[2]Agricultural Biotechnology Center
Plant Biology Institute
Gödöllő
Hungary

Summary

RNA silencing in plants likely exists as a defense mechanism against molecular parasites such as RNA viruses, retrotransposons, and transgenes. As a result, many plant viruses have adapted mechanisms to evade and suppress gene silencing. Tombusviruses express a 19 kDa protein (p19), which has been shown to suppress RNA silencing in vivo and bind silencing-generated and synthetic small interfering RNAs (siRNAs) in vitro. Here we report the 2.5 Å crystal structure of p19 from the *Carnation Italian ringspot virus* (CIRV) bound to a 21 nt siRNA and demonstrate in biochemical and in vivo assays that CIRV p19 protein acts as a molecular caliper to specifically select siRNAs based on the length of the duplex region of the RNA.

Introduction

RNA silencing is a gene inactivation system in which sequence specificity is provided by short RNAs. It was initially identified as a conserved surveillance system that occurs in a broad range of eukaryotic organisms including fungi (quelling), animals (RNA interference [RNAi]), and plants (posttranscriptional gene silencing [PTGS]). RNA silencing acts against molecular parasites, including transposons, transgenes, and viruses and is emerging as a basic gene regulation process that interferes with different layers of endogenous gene expression in most, if not all, eukaryotic cells (reviewed in Baulcombe, 2002a; Hannon, 2002; Voinnet, 2002). RNA silencing is also likely involved in the maintenance of genome stability by regulating heterochromatin formation in the fission yeast (Provost et al., 2002; Volpe et al., 2002) and in plants (Hamilton et al., 2002; Zilberman et al., 2003).

A conserved set of gene products is required for RNA silencing in plants, animals, and fungi (reviewed in Cogoni and Macino, 2000). The molecular mechanism of RNA silencing involves the initial processing of double-stranded RNA (dsRNA) into short (21–26 nt) dsRNA duplexes called small interfering RNAs (siRNAs) (Hamilton and Baulcombe, 1999; Zamore et al., 2000). These siRNAs are produced in *Drosophila* by a nuclease from the ribonuclease III family named Dicer or in plants by Dicer homologs (Bernstein et al., 2001; Ketting et al., 2001; Park et al., 2002). siRNAs are generally characterized by their short length (21–26 nt), 2 nt, 3′ overhanging ends, and 5′ phosphate groups. Upon incorporation of one of the two strands of the siRNA into a ribonucleoprotein complex, the RNA-induced silencing complex (RISC), the siRNA targets mRNAs with extensive, if not complete, sequence complementarity for subsequent degradation (Elbashir et al., 2001a, 2001b; Hammond et al., 2001; Martinez et al., 2002; Zamore et al., 2000).

Most plant viruses have positive sense, single-stranded (ss) RNA genomes (Hull, 2002) replicating via dsRNA intermediates, which are strong inducers of RNA silencing and are believed to be the precursors of viral siRNAs (Ahlquist, 2002). Upon incorporation of these viral-derived siRNAs into RISC, the viral RNA is specifically targeted for degradation (Baulcombe, 1999; Waterhouse et al., 1999) allowing the plant to recover from viral infection. As a counter-defense mechanism, both plant and insect viruses have evolved proteins that suppress RNA silencing (Baulcombe, 2002b; Li et al., 2002; Li and Ding, 2001; Voinnet, 2001) by targeting different steps of the silencing pathway (Li and Ding, 2001). A number of silencing suppressors have been identified from different types of viruses, including positive and negative sense ssRNA and ssDNA viruses (Anandalakshmi et al., 1998; Brigneti et al., 1998; Kasschau and Carrington, 1998; Li and Ding, 2001; Voinnet et al., 1999), but the molecular mechanisms by which suppression occurs are still unclear.

The linear, positive sense ssRNA genome of tombusviruses encodes a 19 kDa protein (p19, ORF 5) that was first characterized as a symptom determinant (Dalmay et al., 1993; Scholthof et al., 1995) and later shown to suppress RNA silencing (Qiu et al., 2002; Qu and Morris, 2002; Silhavy et al., 2002; Voinnet et al., 1999). This protein binds RNA silencing-generated and synthetic 21 nt siRNAs in vitro under stoichiometric conditions (Silhavy et al., 2002). As a result, it has been suggested that p19 binds siRNAs and sequesters them, preventing their incorporation into a RISC. Site-directed mutagenesis studies have characterized several amino acids in the p19 protein that are critical for symptom induction (Chu et al., 2000) and thus could be important for RNA silencing suppressor function via siRNA recognition; however, the mechanism by which p19 selectively recognizes the siRNA silencing signal is still unknown.

Here we present the crystal structure of the *Carnation Italian ringspot virus* (CIRV) p19 protein in complex with a 21 nt siRNA. Our studies reveal how this family of RNA silencing suppressor proteins interacts with and specifically recognizes the siRNA. These structural studies in conjunction with binding assays show that p19 has a high affinity for 21 nt siRNAs with little to no distortion of the standard A form dsRNA structure. Surprisingly, the siRNA's characteristic 2 nt, 3′ overhangs are not necessary for high-affinity binding, but binding is enhanced with siRNAs containing the 5′ phosphate groups. The length of the duplex region of the siRNA is critical for high-affinity binding. CIRV p19 binds tightly

Table 1. Summary of Data Collection, Phasing, and Refinement Statistics

Data Statistics		
Data Set	Native	5BrU
Space Group	$P6_122$	$P6_122$
Unit cell	a = 115.4	a = 115.5
	b = 115.4	b = 115.5
	c = 128.2	c = 128.6
	$\alpha = \beta = 90, \gamma = 120^\circ$	$\alpha = \beta = 90, \gamma = 120^\circ$
Resolution (Å)	2.5	2.6
R_{sym} (%)[a,b]	8.7 (38.1)	11.2 (39.9)
Total reflections (unique)	318939 (17767)	248506 (14971)
Completeness (%)[b]	98.8 (95.4)	92.9 (50.1)
Redundancy[b]	18.9 (7.1)	18.7 (1.0)
$I/\sigma(I)$[b]	34.9 (2.7)	24.5 (2.6)
Detector	MarCCD	MarCCD
X-ray source	SER-CAT 22-ID	SER-CAT 22-ID
Wavelength (Å)	1.0000	0.91920
Phasing Statistics		
Number of Sites		10 (half-occupancy sites)
Anomalous phasing power (acentric reflections)		0.91
R_{cullis} anomalous (acentric reflections)		0.85
Figure of merit		0.30
Refinement Statistics		
R_{cryst} (%)[c]	22.4	
R_{free} (%)[d]	28.9	
Number of protein atoms	2164	
Number of RNA atoms	890	
Number of water molecules	111	
RMSD bond lengths (Å)	0.006	
RMSD bond angles (°)	1.18	
average B-factor (Å^2)		
Protein	41.9	
RNA	40.9	
Solvent	45.4	

[a] $R_{sym} = \Sigma_{hkl}\Sigma_i|I_{hkl,i} - \langle I\rangle_{hkl}|/\Sigma_{hkl}\Sigma_i|I_{hkl,i}|$ where I_{hkl} is the intensity of a reflection and $\langle I\rangle_{hkl}$ is the average of all observations of this reflection and its symmetry equivalents.

[b] Values in parentheses refer to the highest resolution shell.

[c] $R_{cryst} = \Sigma_{hkl}|F_{obs} - F_{calc}|/\Sigma_{hkl}|F_{obs}|$.

[d] R_{free} = R factor for 5% of the reflections that were not used in refinement (Brünger, 1992).

to siRNAs of 20–22 nt, but progressively weaker to siRNAs of 23–26 nt and poorly to a 19 nt siRNA. Although amino acid sequence homologs have not been detected in proteins other than tombusvirus p19s, this mode of recognition may represent a prototype for other siRNA binding proteins in the RNA silencing machinery.

Results and Discussion

Structure of CIRV p19 Bound to an siRNA

We expressed and purified the full-length CIRV p19 protein and obtained single crystals of CIRV p19 in complex with a 21 nt siRNA that diffracted to 2.5 Å resolution. We determined the structure of the complex by single wavelength anomalous dispersion (SAD; Wang, 1985) using a synthetic siRNA with incorporated 5-bromouracil. Statistics for the structure determination are shown in Table 1.

CIRV p19 binds to an siRNA as a dimer with two molecules of p19 per siRNA duplex (Figure 1A). A monomer of CIRV p19 comprises five α helices and a single four-stranded β sheet (Figure 1B). The p19 monomer can be divided into N-terminal (residues 9–48) and C-terminal (residues 55–152) subdomains connected by a short linker (residues 49–54) (Figure 1C). We were unable to build a model for the short linker region between the two subdomains due to poor electron density. This suggests an inherent flexibility of the linker; the lack of RNA or protein contacts may prevent a single conformation from being favored energetically. As a dimer, the N-terminal subdomains of p19 contact the ends of the siRNA duplex, capping what would be the exposed faces of the last basepairs and also contact the 2 nt, 3′ overhanging nucleotides. This subdomain comprises two α helices (α1 and α2) that are connected by a long random coil (residues 18–38). Residues from this subdomain that contact the siRNA are located in the two α helices (Figure 1C). The C-terminal subdomain functions in protein-protein dimerization and dsRNA binding and comprises a four-stranded β sheet and three α helices (α3–α5) that form an $\alpha + \beta$ sandwich. p19 forms a tail-to-tail homodimer with hydrogen bonds between the β4 strands (residues 119–126) from each monomer (Figure 1D) and hydrophobic and salt bridge

interactions between residues in the α5 helices (residues 130–144). The dimerization results in a continuous eight-stranded β sheet forming a concave surface that blankets the dsRNA minor groove (Figure 1E). The conformation of the 19 bp double-stranded region of the siRNA is A form, and there is little to no distortion of the structure due to p19 binding.

A search for structurally homologous proteins using the program DALI (Holm and Sander, 1993) revealed that the topology of the C-terminal subdomain of p19 is similar to that of domain I of protein L1 in the 50S ribosomal subunit (Figure 2A) (Nikulin et al., 2003). The root mean square deviation over 45 equivalent Cα positions in p19 and L1 is 2.0 Å (Figure 2B). A circular permutation is necessary for the topologies to be identical, a commonly observed phenomenon (Jung and Lee, 2001). In domain I of L1, the connection between α1 and β1 must be broken and a connection must be formed between β10 and α1. Furthermore, instead of a short loop, β1 and β8 are connected by the insertion of domain II of L1. The four-stranded β sheets are the most similar in both proteins and each sheet binds to dsRNA. Domain I of L1 binds the dsRNA stem of a hairpin protuberance in the 50S ribosome (Nikulin et al., 2003). While both L1 and p19 bind dsRNA, the dimerization strand in p19 (β4) is eight residues long compared to the homologous strand in L1 (β10), which is only three residues long. The differences in the secondary structural elements explain why L1 does not dimerize in the same manner as p19. L1 binds as a monomer to the 23S rRNA in the low-resolution crystal structure of the 70S ribosome (Yusupov et al., 2001) and to a single stem-loop RNA structure in the high-resolution structure of L1 (Nikulin et al., 2003). Presumably, by forming a dimer, p19 can bind to a longer dsRNA extending over the 19 basepairs of an siRNA. This structural and functional homology provides evidence that residues in the C-terminal portion of p19 form a general dsRNA binding subdomain.

CIRV p19 Recognition of siRNA

CIRV p19 interacts with the siRNA over the length of the molecule. As expected, the contacts between protein and RNA appear to be sequence independent since there are no interactions between the protein and the RNA bases, other than stacking interactions with the last basepairs at each end of the duplex region (see below). The observed contacts can be divided into two classes: phosphate group and end-capping interactions. Interactions with the phosphate groups are made by basic and polar residues from both subdomains of the p19 protein (Figures 1C and 3A). These residues contact the siRNA phosphate groups on one side of the RNA helix (Figure 1A). Interactions with the phosphate groups are localized to the central portion of the RNA duplex and the duplex ends, leaving the intervening duplex regions untouched (Figure 3A). These contacts follow the phase of the RNA helix occurring ~10 bp apart or roughly one turn of the A form helix. There are three contacts with the 2 nt, 3′ overhang in the model: two hydrogen bonds between the sidechain oxygen of Thr40 and both the phosphate group of Ura21 and the O2′ oxygen of Ura20 and a potential hydrogen bond (3.2 Å) between the sidechain nitrogen of Arg43 and the O3′ oxygen of Ura20.

The end-capping interactions are made by two tryptophan residues in the N-terminal subdomain of p19 (Figure 3C). Trp39 and Trp42 from each monomer of p19 form stacking interactions with bases Gua19 and Cyt1, respectively, capping the exposed RNA basepairs at each end of the duplex. In addition, the imino nitrogen of Trp42 forms a hydrogen bond with the 5′ phosphate group, indicating a possible preference for a 5′-phosphorylated siRNA. Arg43 and Asn46 stack with Trp39 and Trp42, respectively, thereby preventing the surface exposure of the hydrophobic tryptophans. Arg43 is absolutely conserved among tombusvirus p19s, and Asn46 is either Asn or His (Figure 1C). The importance of this stacking interaction for the stability of p19 from the closely related *tomato bushy stunt virus* (TBSV) was demonstrated by Chu et al. with the mutation of Arg43 to tryptophan (which could stack with Trp39, but would result in an exposed tryptophan residue), resulting in viruses that did not produce the necrosis phenotype observed with wild-type virus (Chu et al., 2000). Because these end-capping interactions occur at both ends of the RNA duplex, they result in p19 forming what appears to be a caliper, clasping the duplex portion of the siRNA. This suggests that optimal p19 binding of siRNA is dependent on the length of the duplex region of the siRNA.

The residues that contact the phosphate groups of the siRNA are fairly well conserved among p19s from other tombusviruses, but surprisingly are not absolutely conserved (Figure 1C) and include some nonconservative substitutions (e.g., substitution of Gly for Arg11 and substitution of Cys for Arg18). These p19 proteins still retain at least six of nine phosphate-interacting residues, so we would not anticipate a severe effect on siRNA binding. Perhaps the p19 proteins that lack some of these electrostatic interactions bind with lower affinity than CIRV p19 and other p19s that retain all nine of the phosphate group-interacting residues. More surprising than the lack of complete conservation of phosphate-interacting sidechains is the observation that neither of the two end-capping tryptophans is absolutely conserved (Figure 1C). However, in all p19 sequences detected in a PSI-BLAST (Altschul et al., 1997) search of the protein database, at least one of the two tryptophans is conserved (usually Trp42, which interacts with the 5′ phosphate group) while the other may be substituted with arginine, leucine, or serine.

The Role of Tryptophan End-Capping Residues in Silencing Suppression

Previously it was demonstrated that lack of p19 in tombusvirus infection leads to plant recovery from virus infection due to the activation of RNA silencing (Szittya et al., 2002). In order to investigate the importance of the end-capping tryptophans of p19 for silencing suppression, we introduced mutations into the p19 coding sequence of the CIRV genome to change one or both of the tryptophan residues. Mutations made to CIRV p19 to remove one or both tryptophans show attenuation in the wild-type virus-induced lethal necrosis phenotype in virus-infected *Nicotiana benthamiana* plants (Figures 4A and 4B). Substituting arginine, a residue that may still stack on the exposed RNA base, for either of the two tryptophans has a mild effect on the severe symptoms

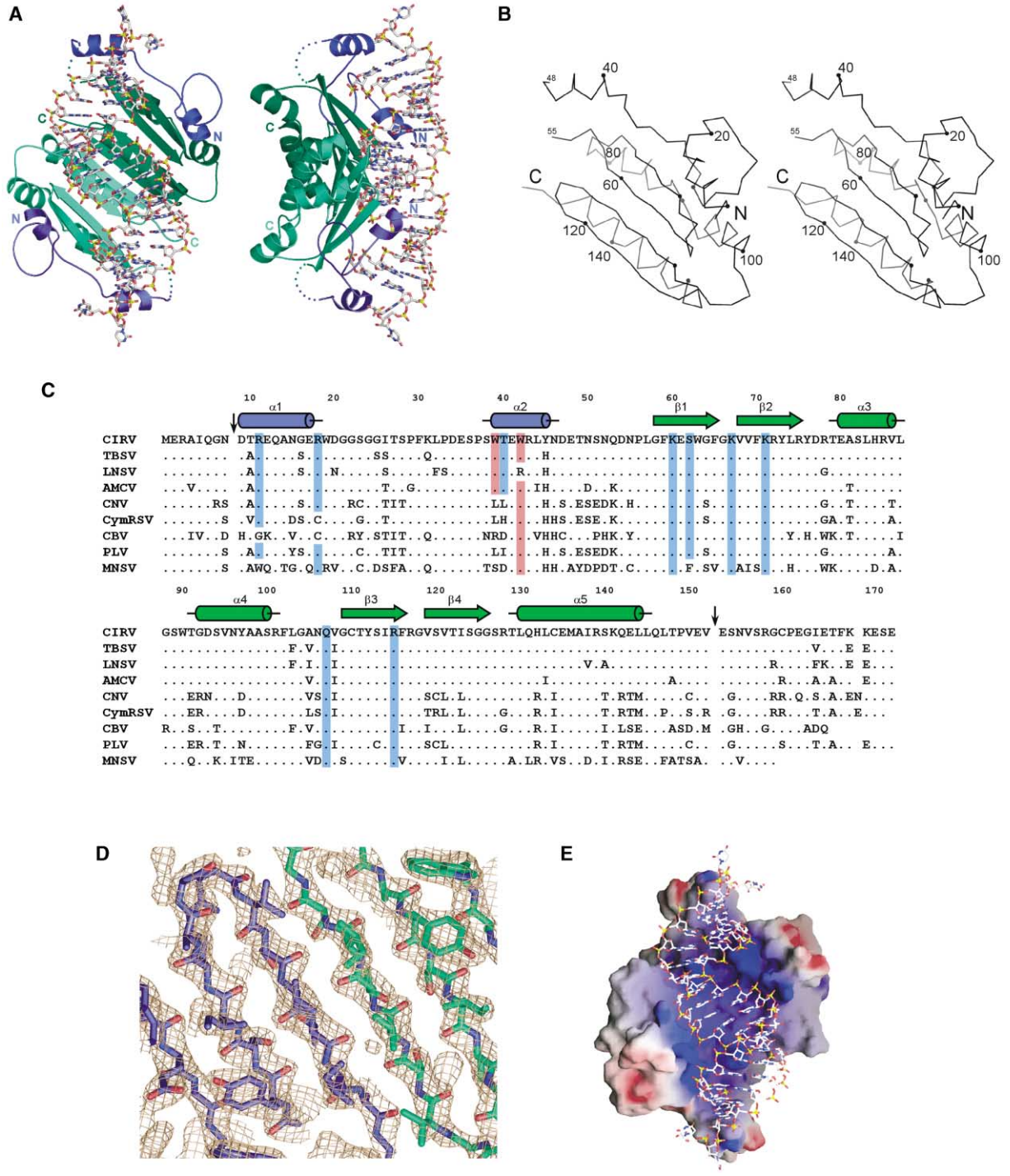

Figure 1. Crystal Structure of CIRV p19 in Complex with a 21 nt siRNA and Conservation of p19 Protein Sequences

(A) Two orientations (related by a 90° rotation about the vertical axis) of the CIRV p19:siRNA complex. The siRNA is rendered as sticks. Ribbon diagram of the p19 dimer colored by N-terminal (blue and slate) and C-terminal (dark green and green) subdomains. The disordered linker connecting the subdomains is rendered as spheres. The protein N and C termini are indicated.

(B) Stereo diagram of a Cα trace of the structure of a CIRV p19 monomer. Every tenth Cα atom is indicated with a black sphere. Every twentieth Cα atom is labeled. Residues 48 and 55 are labeled to show the start and stop of the disordered linker between the N-terminal and C-terminal subdomains.

(C) Alignment of the amino acid sequences of p19s from representative tombusvirus family members. The sequences of *Carnation Italian ringspot virus* (accession number NP_612584), *Tomato bushy stunt virus* (AAC32734), *Lettuce necrotic stunt virus* (CAC01269), *Artichoke mottled crinkle virus* (P15960), *Cucumber necrosis virus* (NP_040957), *Cymbidium ringspot virus* (NP_613264), *Cucumber Bulgarian virus* (NP_835257), *Pear latent virus* (NP_835243), and *Maize necrotic streak virus* (AAG21219) are shown. The amino acid numbering and secondary structural elements (colored slate for N-terminal and green for C-terminal subdomains) observed in the crystal structure are shown above the alignment. Arrows above the alignment and near the N and C termini indicate the extent of p19 modeled in the electron density. Residues

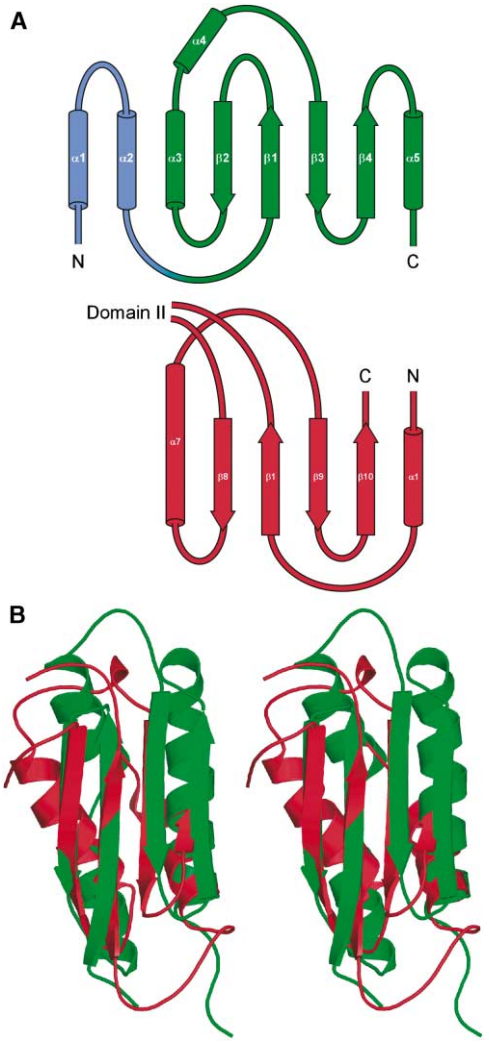

Figure 2. Topology and Structural Alignment of CIRV p19 and Domain I of Protein L1

(A) Topology of p19 (green [C-terminal subdomain] and slate [N-terminal subdomain]) and domain I of protein L1 of the 50S ribosomal subunit (red).

(B) Stereo diagram of the structural alignment of the C-terminal subdomain of p19 (green) with domain I of the high-resolution crystal structure of protein L1 (red; PDB accession 1MZP [Nikulin et al., 2003]).

caused by virus infection of the plant. This suggests that those tombusvirus p19 proteins that lack one of the tryptophans may retain RNA silencing suppression activity. In fact, *Cymbidium ringspot virus* (CymRSV) p19 has a leucine in place of Trp39 and has been shown to be active as an RNA silencing suppressor (Silhavy et al., 2002). Substituting arginine for both tryptophans in the p19 sequence, however, more significantly attenuates the severe symptoms of CIRV and the plants partially recover. Finally, substituting glycine for Trp39 results in plant recovery from mutant virus infection, indicating the lack of silencing suppression. Thus the lack of a sidechain to make a stacking interaction is highly deleterious for suppressor activity. To be sure that the above observed symptom attenuation was a consequence of the altered ability of p19 mutants to suppress silencing, we also incubated a plant infected with each of the p19 mutant viruses at 15°C where silencing is inactive (Szittya et al., 2003). All mutant viruses failed to show recovery (data not shown). Instead they caused severe symptoms similar to wild-type virus, confirming that the attenuated symptoms of p19 mutants are related to the altered suppressor activity of mutant p19s.

To examine whether the tryptophan mutations interfere with suppression of transgene-induced RNA silencing, wild-type *N. benthamiana* plants were infiltrated with an *Agrobacterium tumefaciens* carrying a green fluorescent protein (GFP) gene construct (35S-GFP) or coinfiltrated with *A. tumefaciens* carrying 35S-GFP and with another *A. tumefaciens* expressing the p19 mutant protein of interest. Infiltration of wild-type *N. benthamiana* leaves with a strain of *A. tumefaciens* carrying 35S-GFP results in transient GFP expression but also leads to induction of GFP RNA silencing (Johansen and Carrington, 2001; Silhavy et al., 2002). RNA silencing, manifested in the reduction of GFP fluorescence, results in decline in GFP mRNA levels and accumulation of GFP-specific siRNAs in the infiltrated patches (Figures 4C and 4D). Coexpression of GFP and wild-type CIRV p19 by agroinfiltration suppresses GFP RNA silencing and results in a prolonged green fluorescence of GFP (Figure 4C), high levels of GFP mRNA, and lack of GFP siRNA accumulation (Figure 4D). The level of GFP silencing suppression in the agroinfiltration assays correlates with the symptom severity caused by tryptophan mutant viruses. RNA silencing suppression was reduced slightly relative to wild-type in the W39R and W42R single mutants (Figures 4C and 4D). However, we observed larger reductions in suppression in the W39/42R double mutant and W39G single mutant (Figure 4C), indicating a reduction of activity of the mutant p19 proteins. The mutant p19 proteins were produced at similar levels; however, the GFP-derived siRNAs accumulated to higher levels while GFP mRNA levels were significantly lower than in the control wild-type p19 infiltration (Figure 4D). These results support the conclusion drawn from the p19 mutant virus infection assays that the observed differences in viral symptoms or in the different silencing suppression level of GFP and p19 coexpression experiments are the consequence of altered suppressor activity of mutant CIRV p19.

Mutational analysis of numerous basic residues in TBSV p19 assayed by the viral-induced lethal necrosis phenotype have been studied in three different plant

that contact phosphate groups in the siRNA are labeled in blue and residues that stack on the siRNA duplex end are labeled in red.

(D) Electron density at the dimer interface. Ball-and-stick representation of the β sheet dimer interface is shown with carbon atoms from monomer A colored slate and carbon atoms from monomer B colored green. A $2F_o$-F_c electron density map contoured at 1.5σ is superimposed.

(E) Electrostatic surface representation of p19. Regions of positive potential are blue and regions of negative potential are red at the 10 kT/e level. Figures 1A, 1B, 1D, 2B, 3B, and 3C are rendered with PYMOL (DeLano, 2002). Figure 1E is rendered with GRASP (Nicholls et al., 1991).

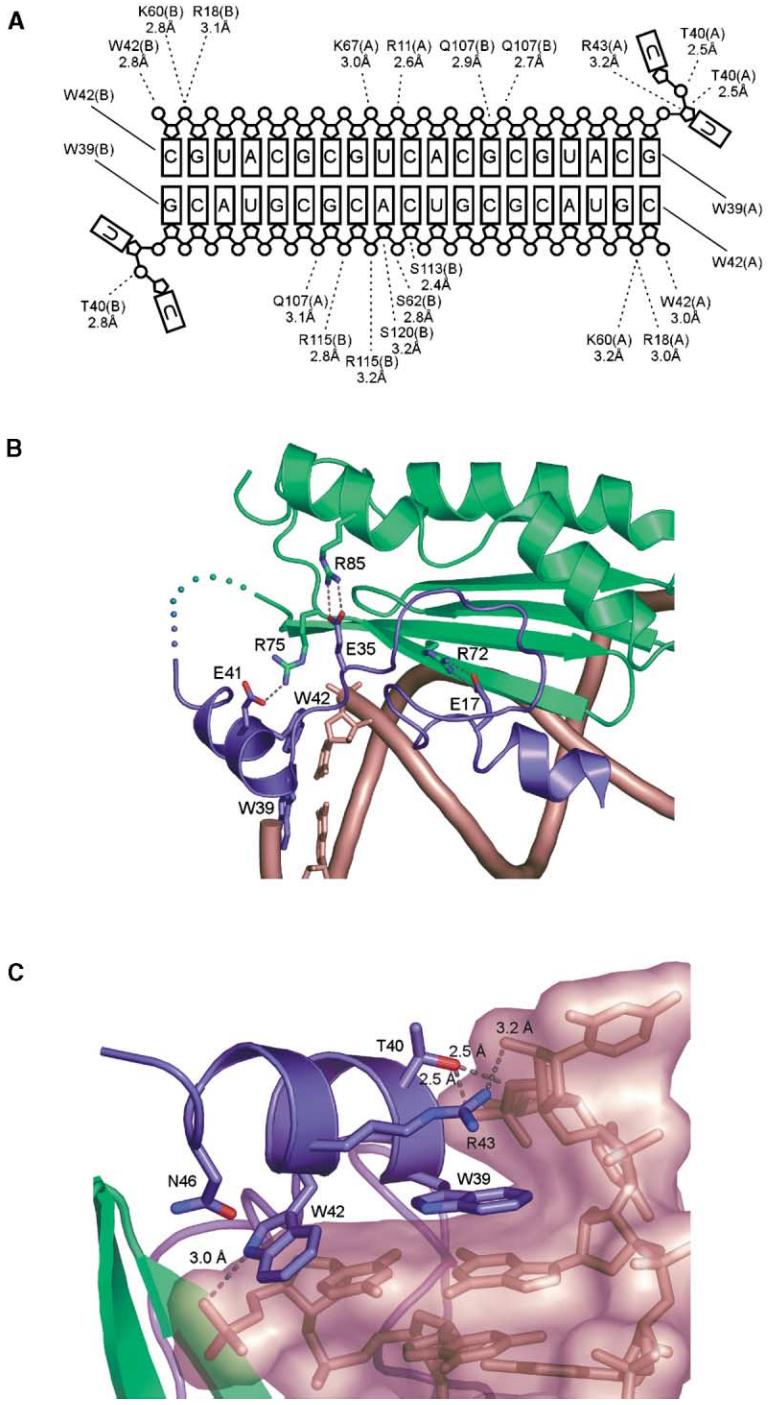

Figure 3. Protein:RNA Interactions

(A) Schematic representation of protein:RNA contacts from NUCPLOT (Luscombe et al., 1997) using a 3.2 Å cutoff. Contacts between amino acid residues and RNA phosphate/sugar groups are shown as dashed lines, while stacking interactions are shown as solid lines.

(B) Salt-bridge interactions between Arg72, Arg75, and Arg85 on the C-terminal subdomain with residues Glu17, Glu41, and Glu35, respectively, on the N-terminal subdomain. The siRNA backbone is rendered as a ribbon.

(C) Interaction of residues Trp39 and Trp42 in the N-terminal subdomain with the siRNA duplex end (rendered as a transparent surface). Interaction of Asn46 and Arg43 with Trp42 and Trp39, respectively, is also shown.

Figures in (B) and (C) show the N-terminal subdomain colored slate, C-terminal subdomain colored green, hydrogen bonds or salt bridge interactions rendered as dashed gray sticks, and siRNA colored tan.

species and compared to wild-type TBSV p19 (Chu et al., 2000). Three mutations, R72G, RR75-78GG, and R85G, displayed the greatest reduction in the lethal necrosis phenotype. None of these residues in CIRV p19, Arg72, Arg75, and Arg85, contact the siRNA but rather form salt bridges to Glu17, Glu35, and Glu41, respectively (Figure 3B). All of these salt bridges occur at the interface between the N-terminal and C-terminal subdomains in p19 and likely facilitate the positioning of the RNA end-capping tryptophan residues with respect to the dsRNA binding portion of p19. In addition, the salt bridge involving Arg72 and Glu17 is buried, and as a result, the R72G mutation would result in a buried charged residue (Glu17), which likely impacts the structural integrity of the protein as suggested by Chu et al. (2000). Two other mutations in conserved amino acids, K60A and K71A, show decreases in the lethal necrosis phenotype in two of the three species of the plants tested. These amino acids correspond to Lys60 and Lys71 in CIRV p19 and are involved in salt bridges to the RNA phosphate back-

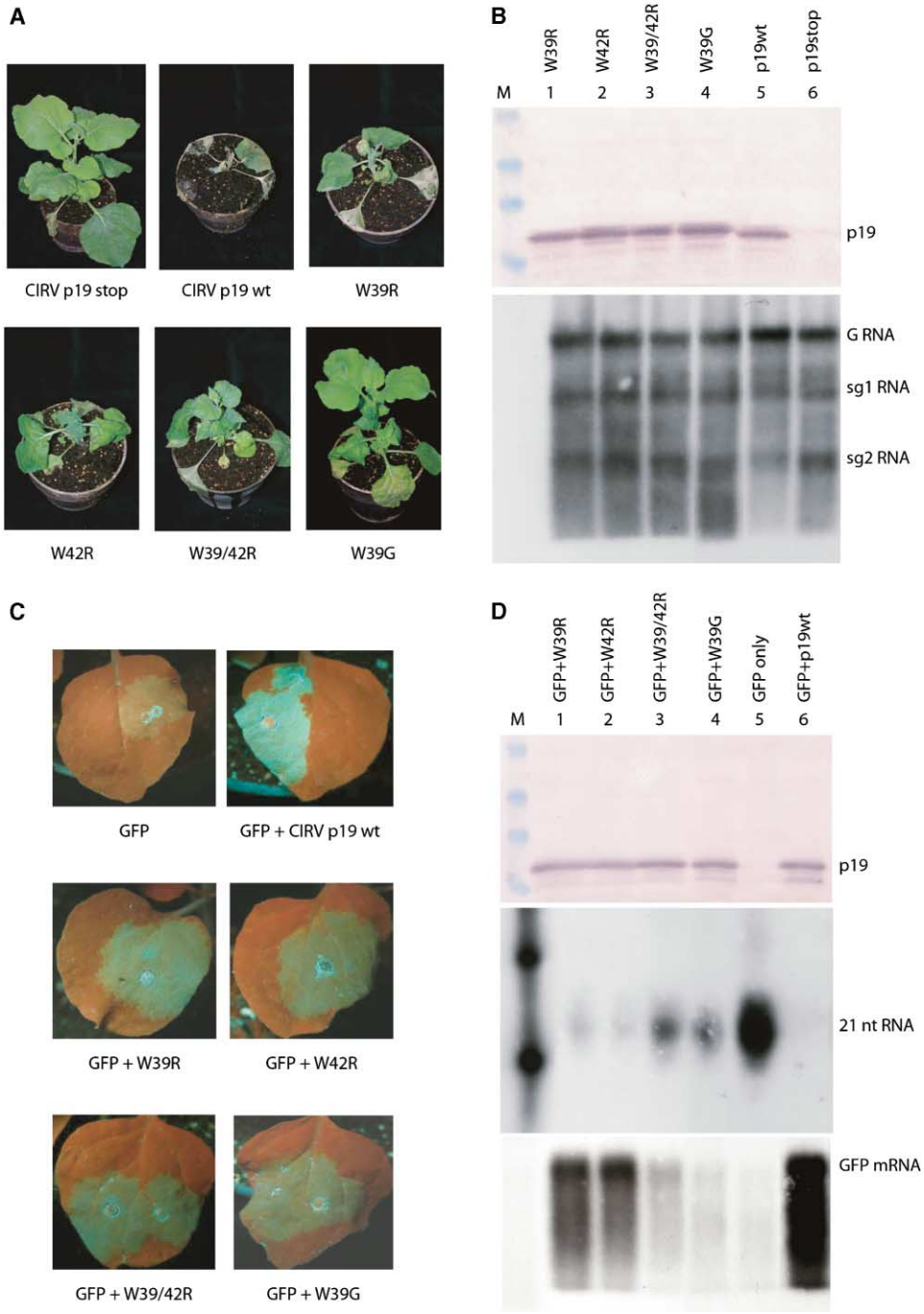

Figure 4. The Effects of CIRV p19 Mutation on Symptom Development, Viral RNA Accumulation, and Transgene-Induced RNA Silencing

(A) Symptoms of plants infected with CIRV expressing wild-type (wt), mutant (W39R, W42R, W39/42R, or W39G), or no (stop) p19 protein. Photos were taken 4 weeks post-inoculation.

(B) Western blot of total protein (top) and RNA gel blot analysis of virus-specific RNAs (bottom) extracted from wild-type, stop, and mutant CIRV p19 inoculated leaves of *N. benthamiana* plants shown in (A). Genomic (G) and subgenomic (sg1 and sg2) viral RNAs are labeled in the RNA gel blot analysis.

(C) Leaves of wild-type *N. benthamiana* infiltrated with Agrobacterium carrying 35S-GFP or coinfiltrated with Agrobacterium carrying 35S-GFP and wild-type or mutant 35S-CIRV p19. Silencing of GFP results in red fluorescence (auto fluorescence of chlorophyll) whereas silencing suppression results in green fluorescence. Photographs were taken 6 days post-inoculation of UV-illuminated leaves.

(D) Western blot of total protein (top) and RNA gel blot analysis of GFP-specific 21 nt RNA (middle) and GFP mRNA (bottom). Protein and RNA extractions were performed at 6 days post inoculation.

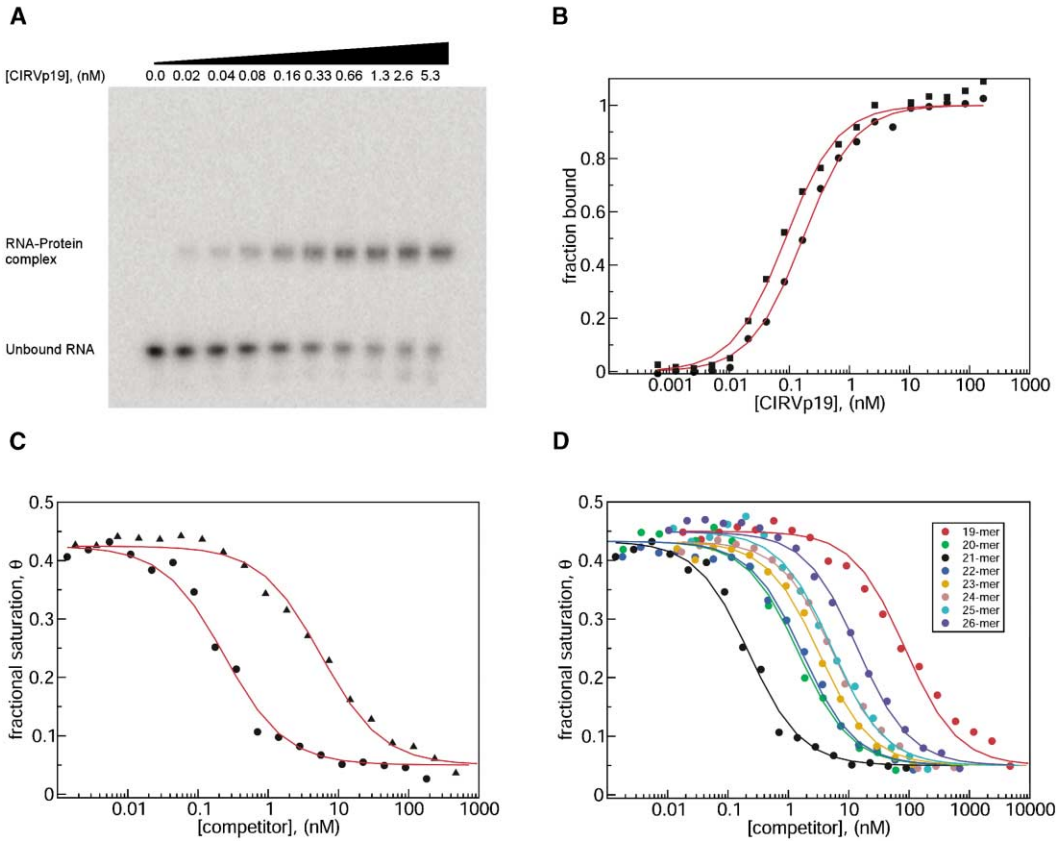

Figure 5. Analysis of the Affinity and Specificity of CIRV p19 for siRNAs

(A) Representative gel mobility shift assay performed with 21-mer siRNA with 2 nt, 3′ overhangs and 5′ phosphate groups at fixed concentration with varying concentrations of CIRV p19, showing the points from 0.02–5.3 nM protein concentration. No binding was detected for 21 nt ssRNA in the range of substrate concentrations tested (<2 μM) showing that p19 binds specifically to duplex RNA (data not shown).

(B) Representative analysis of direct binding equilibrium data with CIRV p19 binding to 21-mer siRNA including 2 nt, 3′ overhangs and 5′ phosphate groups (circles) or 19-mer siRNA including 5′ phosphate groups and no overhangs (squares). Best-fit binding isotherms (red) are shown assuming one dimer of wild-type CIRV p19 binds a single siRNA.

(C) Competition analysis for 21-mer siRNA binding to CIRV p19. Competition was with unlabeled 21-mer siRNA with 5′ phosphate groups (circles) and without 5′ phosphate groups (triangles). Data were fit assuming one siRNA binds one dimer of CIRV p19.

(D) Analysis as in (C) for competition with unlabeled siRNAs of various lengths shown inclusive of the 2 nt, 3′ overhangs and 5′ phosphate groups.

bone, suggesting that the loss of these interactions may impact suppressor activity.

CIRV p19 Affinity and Specificity for siRNAs

The characteristics of the siRNA cleavage products of the Dicer family of ribonuclease III enzymes include RNA length (~21–26 nt) and the presence of both 5′ phosphate groups and 2 nt, 3′ overhanging ends (Elbashir et al., 2001b; Zamore et al., 2000). Further studies support this functional anatomy by showing that siRNAs with these characteristics are the most efficient at RNA silencing (Elbashir et al., 2001c; Nykanen et al., 2001). In order to examine the characteristics of siRNAs that are important for recognition by p19, we determined the affinity of p19 for siRNA and its specificity for each of the characteristics of siRNA using direct and/or competition binding assays, as appropriate.

The structure of the CIRV p19:siRNA complex suggests that CIRV p19 would have a high affinity for 21 nt siRNA based on the interaction of the end-capping tryptophan residues with the basepairs on each end of the siRNA and the numerous hydrogen bond and salt bridge interactions with the RNA phosphate groups. Direct measurement of the absolute apparent dissociation constant (K_d) for CIRV p19 revealed a high affinity for 21-mer siRNA (19-mer duplex with 5′ phosphate groups and 2 nt, 3′ overhangs): 0.17 ± 0.02 nM (Figure 5A and Table 2). Previous studies using wild-type CymRSV-infected plants have shown that most of the siRNAs in the plant-infected cells are complexed with p19 (L. Lakatos et al., submitted), while in plants infected with CymRSV that do not express p19 (Cym19stop), the siRNA accumulates in the free form and systemic silencing develops. Thus, it is likely that the high affinity of p19 for siRNAs sequesters the free siRNAs and prevents the silencing signal from being incorporated into other effector protein complexes (e.g., RISC).

We observed three hydrogen bonds in our model between p19 and the 2 nt, 3′ overhanging ends; thus, we were curious whether the overhanging nucleotides are required for p19 binding. In our structure, the overhangs are involved in crystal packing contacts, so in solution,

Table 2. Binding of CIRV p19 to ssRNA, dsRNA, and siRNA

Name	Sequence	K_d (nM)	K_{rel}
21-mer	5′ pCGUACGCGGAAUACUUCGAUU 3′ 3′ UUGCAUGCGCCUUAUGAAGCUp 5′	0.17 ± 0.02	1
21-mer ssRNA	5′ pCGUACGCGGAAUACUUCGAUU 3′	>2000	
19-mer (w/o 2-nt 3′)	5′ pCGUACGCGGAAUACUUCGA 3′ 3′ GCAUGCGCCUUAUGAAGCUp 5′	0.08 ± 0.02	
21-mer (w/o 5′-p)	5′ CGUACGCGGAAUACUUCGAUU 3′ 3′ UUGCAUGCGCCUUAUGAAGCU 5′		23
19-mer	5′ pCGUACGCGGAAUACUUCUU 3′ 3′ UUGCAUGCGCCUUAUGAAGp 5′		320
20-mer	5′ pCGUACGCGGAAUACUUCGUU 3′ 3′ UUGCAUGCGCCUUAUGAAGCp 5′		5
22-mer	5′ pCGUACGCGGAAUACUUCGAGUU 3′ 3′ UUGCAUGCGCCUUAUGAAGCUCp 5′		6
23-mer	5′ pCGUACGCGGAAUACUUCGAAGUU 3′ 3′ UUGCAUGCGCCUUAUGAAGCUUCp 5′		22
24-mer	5′ pCGUACGCGGAAUACUUCGAAAGUU 3′ 3′ UUGCAUGCGCCUUAUGAAGCUUUCp 5′		22
25-mer	5′ pCGUACGCGGAAUACUUCGAAAUGUU 3′ 3′ UUGCAUGCGCCUUAUGAAGCUUUACp 5′		37
26-mer	5′ pCGUACGCGGAAUACUUCGAAAUGCUU 3′ 3′ UUGCAUGCGCCUUAUGAAGCUUUACGp 5′		75

K_d is the upper bound of the dissociation constant as measured by direct binding gel mobility shift assays and is uncorrected for percent active protein. K_{rel} is the affinity of the CIRV p19 for siRNA, relative to the affinity for 21-mer with 5′ phosphates and 2 nt, 3′ overhangs as measured by competition binding electrophoretic mobility shift assays.

p19 may make additional, biologically significant interactions with the overhangs. We therefore tested in direct binding assays how well p19 binds to a 19 nt RNA duplex with blunt ends and found that the 2 nt, 3′ overhangs are not required for high-affinity binding, suggesting that the observed contacts with the overhangs may not be stable in solution (Figure 5B). On the contrary, there is a slight improvement in binding without the 2 nt, 3′ overhangs (K_d = 0.08 ± 0.02 nM). Prior to binding by p19, the two overhanging nucleotides are likely stacked with the end basepair to prevent solvent exposure of the hydrophobic base planes of the RNA. Thus, the slightly higher K_d for binding the siRNA with overhanging ends may be due to the additional energy required to unstack the overhanging bases and expose the end base pair of the siRNA during association and re-stack the bases during dissociation of the complex in equilibrium. This result is contradictory to the interpretation of previous results that concluded that the 2 nt, 3′ overhanging ends are important for binding (Silhavy et al., 2002); however, those experiments, performed under stoichiometric conditions, utilized siRNAs with 17 or 21 nt duplex regions, and this change in length of the duplex region likely affected binding (see below).

We also observed one contact with each of the 5′ phosphate groups of the siRNA (Figure 3A). In order to determine the importance of the 5′ phosphate groups for binding by p19, we determined the relative dissociation constants of siRNAs with and without the 5′ phosphate groups using an equilibrium competition assay. The results are shown in Table 2 using a 21 nt siRNA with 5′ phosphate groups as the reference. When the 5′ phosphate group is removed, the affinity of p19 for siRNA is reduced 23-fold with respect to a 21-mer with 5′ phosphate groups (Figure 5C). Structurally, this result is somewhat surprising given the limited interaction of p19 with the 5′ phosphate group (Figure 3C). Perhaps interaction with the phosphate group is needed to position the tryptophan sidechains, both located on α2, with respect to the duplex end for capping. The phosphate group protrudes and can act as a lip to lock the tryptophan residues in place over the duplex end. Biologically, this result is not surprising since Dicer-cleaved dsRNAs contain a 5′ phosphate group (Elbashir et al., 2001b), the 5′ phosphate group is necessary for RNA silencing, and dsRNAs, including siRNAs, without 5′ phosphates are rapidly phosphorylated in *Drosophila* lysate and perhaps in vivo (Nykanen et al., 2001).

Our structure also suggested that the tryptophan capping interactions formed by the p19 dimer might form a caliper on the double-stranded region of the siRNA and measure the length of the siRNA. Thus we tested the ability of p19 to bind siRNAs of different length. We used siRNAs between 19 and 26 nt (17-mer to 24-mer duplex regions with 2 nt, 3′ overhangs) in competition with a 21 nt siRNA (Figure 5D). p19 has the highest affinity for 21-mer siRNA with slight decreases in affinity when one basepair is added or removed, 6-fold or 5-fold, respectively (Table 2). The largest decrease in binding is seen with a 19-mer (removal of a second basepair) resulting in a sharp dropoff in affinity (320-fold). The affinity also decreases significantly, as the duplex region is lengthened, but more gradually than shortening the siRNA. At the longest siRNA length tested (26-mer), the affinity is 75-fold lower than for the 21-mer, approaching the low affinity of the shorter 19-mer siRNA.

In plants, two classes of siRNAs of 21–22 and 24–26 nt are produced (Hamilton et al., 2002; Mallory et al., 2002; Tang et al., 2003). The shorter and longer classes of siRNAs are proposed to have different functions in vivo; the shorter class triggers RNA silencing by degrading complementary mRNA targets, and the longer are responsible for systemic silencing, retrotransposon silencing, and methylation of homologous DNA. There is

also evidence that the distinct classes of siRNA are generated by different Dicer-like enzymes (Tang et al., 2003). The presence of the two classes of siRNAs in plants and the higher affinity of p19 for siRNAs of ~21 nt suggests that p19 preferentially binds the shorter class of siRNAs and would thus have a greater effect on mRNA degradation pathways than on retrotransposon silencing or DNA methylation. Although we do not know the in vivo concentration of p19, and thus it is possible that p19 is present at sufficiently high concentrations to bind both short and long classes of siRNAs, only ~21 nt siRNAs are coimmunopreciptated with p19 (L. Lakatos et al., submitted), and it seems consistent with the function of p19 to protect the viral genome from destruction while sparing other cellular processes. In addition, p19 expressed in the nucleus or cytoplasm had no effect on the methylation of nopaline synthase promoter DNA, suggesting that p19 does not bind to or interfere with long siRNA-directed processes in vivo (Papp et al., 2003).

Our structure suggests that p19 recognizes siRNAs in a sequence-independent manner, and p19 has been demonstrated to suppress RNA silencing in *Drosophila* lysates (L. Lakatos et al., submitted). Thus, p19 has the potential to be used as a tool to understand the mechanism of RNA silencing in heterologous systems. In eukaryotes, including plants, RNA silencing also plays an important role in micro(mi)RNA controlled endogenous gene regulation (reviewed in Bartel and Bartel, 2003). The ability of p19 to specifically bind silencing generated ds siRNAs both in vitro (Silhavy et al., 2002) and in planta (Lakatos and Burgyán, unpublished) raises the possibility that p19 could interfere with any RNA silencing pathway with ds siRNA intermediates. Recent reports suggest that a short-lived double-stranded intermediate precedes the incorporation of mature single-stranded miRNAs into RISC complexes (Bartel and Bartel, 2003; Schwarz et al., 2003) and transgenic *Arabidopsis* expressing p19 displayed an altered phenotype and miRNA accumulation (Papp et al., 2003), implying that p19 may also interfere with miRNA-mediated pathways.

Experimental Procedures

Protein Expression and Purification

Full-length *Carnation Italian ringspot virus* (CIRV) p19 (Burgyán et al., 1996) was expressed as a GST fusion protein in *E. coli* strain BL21(DE3) at 22°C for 20 hr. Bacterial pellets were resuspended in phosphate-buffered saline (PBS, 137 mM NaCl, 2.7 mM KCl, 4.3 mM $Na_2HPO_4 \cdot 7H_2O$, 1.4 mM KH_2PO_4, 1 mM tris(2-carboxyethyl) phosphine hydrochloride (TCEP), pH 8.0) and lysed by sonication in a dry ice/ethanol bath. The fusion protein was purified from the soluble fraction of lysate by incubating with glutathione agarose resin (Sigma, 1 ml resin/2 liter culture) for 15 min at 4°C. The resin was washed with PBS, then with PBS supplemented with 0.5 M NaCl, with cleavage buffer (20 mM Tris-HCl, 0.15 M NaCl, 1 mM TCEP, pH 7.4), and finally with cleavage buffer supplemented with 2.5 mM $CaCl_2$. The resin was incubated with 1 U of thrombin (Novagen) for each 1 ml of resin overnight at 4°C. After cleavage, the liberated p19 protein was collected. p19 was further purified on a Resource Q anion exchange column (Amersham Biosciences). For crystallization, the sample was chromatographed on a Superdex 200 gel filtration column (Amersham Biosciences). CIRV p19 eluted as a dimer (data not shown). The dimeric fractions of CIRV p19 were pooled and concentrated to ~7–12 mg/ml.

Crystallization and Data Processing

RNA oligonucleotides (Dharmacon Research) were annealed at 90°C for 1 min followed by a slow cooling to room temperature at a rate of 1°C/5 min to select for duplex siRNA over hairpin RNA species. The siRNA was then combined with CIRV p19 at 1:1 molar ratio and incubated on ice for 30 min. Crystals were grown from hanging drops by the method of vapor diffusion. One μl of a 0.2 mM solution of protein:RNA complex was mixed with 1 μl of reservoir solution (22.5% (w/v) PEG MME 2000, 100 mM sodium acetate, pH 4.6, 200 mM ammonium sulfate) and equilibrated over the reservoir solution at 4°C. CIRVp19:siRNA crystals grew as hexagonal rods with dimensions of 0.07 mm × 0.07 mm × 0.25 mm within 2–4 days. Crystals were obtained of CIRV p19 with a 21 nt siRNA formed from a near palindromic oligonucleotide resulting in a central C-C mismatch (native) and a 21 nt siRNA formed from two oligonucleotides substituted with 5-bromouracil at a total of five positions (5BrU). The sequence of the oligonucleotide used to form the near palindromic duplex siRNA is 5′-pCGUACGCGUCACGCGUACGUU-3′, and the sequences containing the 5-bromouracil-substituted oligonucleotides are 5′-pCG[5BrU]ACGCGGAA[5BrU]ACUUCGAUU-3′ (strand 1) and 5′-pUCGAAG[5BrU]AU[5BrU]CCGCG[5BrU]ACGUU (strand 2).

Prior to data collection, crystals were transferred to reservoir solution supplemented with 9% (v/v) ethylene glycol and flash cooled to −180°C in liquid nitrogen. Diffraction data for the native CIRV p19:siRNA complex and the 5BrU CIRV p19:siRNA complex were collected to 2.5 Å and 2.6 Å resolution, respectively, at beamline 22-ID SER-CAT at the Advanced Photon Source at Argonne National Laboratory using a MarCCD detector (Table 1). The native dataset was processed with DENZO and SCALEPACK, and the 5BrU dataset was processed with HKL-2000 (Otwinowski and Minor, 1997).

Structure Determination and Refinement

The structure of the CIRV p19:siRNA complex was determined by single-wavelength anomalous dispersion (SAD) (Wang, 1985) using a dataset collected at the absorption peak of Br. Heavy atom sites were located with the program CNS (Brünger et al., 1998). Because a dimer of CIRV p19 (monomers A and B) binds to an siRNA with a 2-fold noncrystallographic symmetry axis coincident with the siRNA pseudo-dyad, the siRNA can bind in either of two positions, with the 5′ end of strand 1 bound to either monomer A or monomer B. However, the 5-bromouracil positions are not 2-fold symmetric about the pseudo-dyad, thus the five full-occupancy Br sites in the siRNA appear as ten half-occupancy sites in the crystal asymmetric unit. Heavy atom positions were refined and the phases were calculated with SHARP (de la Fortelle and Bricogne, 1997) to 3.0 Å resolution. An initial round of density modification was carried out with SOLOMON (Abrahams and Leslie, 1996). A final round of density modification including noncrystallographic symmetry averaging and phase extension to 2.6 Å was performed with DM (Collaborative Computational Project, 1994). Model building was carried out with the program O (Jones et al., 1991). The resulting atomic model was refined against the native data set using reflection intensities and the maximum likelihood target function in the program CNS (Brünger et al., 1998). The model of CIRV p19 includes residues 9–152 of p19 monomer A (Arg128 is truncated and loop residues 49–54 are deleted due to poor, weak density) and 9–149 of monomer B (Arg101 and 128 are truncated and loop residues 49–54 are deleted due to poor, weak density). There was some static disorder in the siRNA resulting in a need to model the RNA with two siRNAs at 0.6 and 0.4 occupancies to account for multiple conformations.

Model quality was assessed using the program MOLPROBITY (Lovell et al., 2003). All ϕ-ψ torsion angles are within allowed regions of the Ramachandran with the exception of residue 23 of monomer B, which is located in a poorly ordered loop, and more than 88% are in the most favored regions.

Electrophoretic Mobility Shift Assays

RNA oligonucleotides were radiolabeled in 50 pmol quanitities with 0.3 μM [γ-^{32}P] ATP (PerkinElmer Life Sciences) and 20 U of T4 polynucleotide kinase (New England Biolabs Inc.) according to the manufacturer's directions. A synthesized 5′-phosphorylated complementary strand was added to the inactivated kinase reaction and

the oligos were annealed at 90°C for 1 min followed by a slow cool at a rate of 1°C/3 min. The siRNA duplex was purified on a 20% polyacrylamide tris-borate-ethylenediaminetetraacetic acid (TBE) gel (Novex, Invitrogen Inc.). Protein solutions were diluted in buffer containing 20 mM Tris-HCl (pH 7.0), 1 mM TCEP, and 0.02% (w/v) Tween-20. For direct binding experiments, CIRV p19 was titrated against <2.5 pM radiolabeled siRNA in binding buffer containing 20 mM Tris-HCl (pH 7.0), 1 mM EDTA, 1 mM TCEP, 100 mM NaCl, and 0.02% Tween-20. For competition experiments, synthesized 5′-phosphorylated oligonucleotides were annealed as in the labeling procedure to form competitor RNA. Competitor siRNAs were titrated against <2.5 pM radiolabeled 21-mer siRNA with 2 nt, 3′ overhangs and 0.7 nM CIRV p19 (concentration at which ~80% of the siRNA was bound in the direct binding experiment) in binding buffer. Binding reactions were incubated at room temperature for 45 min–1 hr, adjusted to 7.5% (w/v) Ficoll 400, and a portion of the reaction analyzed by electrophoresis at a constant 100 V for 45 min through a 6% TBE DNA retardation gel (Novex, Invitrogen Inc.) in 0.5X TBE. The gels were then dried, exposed to a storage phosphor screen for 1–5 days, and bands corresponding to bound and free radiolabeled probe were quantified with a Molecular Dynamics Typhoon phosphorimager (Amersham Biosciences) and ImageQuant software. All competition experiments were performed in triplicate. The data from the direct binding experiments were fit to a rectangular hyperbola and the competition binding experiments were fit to the equation describing fractional saturation of the radiolabeled species in the context of competitive binding of two ligands to a protein (Lin and Riggs, 1972; Weeks and Crothers, 1992).

Preparation of p19 Mutant Viruses, In Vitro RNA Transcription, and Plant Inoculation

Site-directed mutants were introduced into the p19 encoding region (between 3872 and 4390 nt) of the CIRV genome by PCR using the appropriate primer set for each of the following mutants and confirmed by DNA sequencing. For the CIRV-p19stop mutant, two stop codons were introduced in the third and sixth codon positions of ORF5, which encodes the p19 protein, in the full-length cDNA clone of CIRV. For the p19 mutants of W39R, W42R, W39/42R, W39G, and p19stop, the modifications did not alter the amino acid sequence of the p22 movement protein encoded by ORF4. In vitro transcripts of wild-type CIRV and p19 mutants were prepared and used to inoculate *N. benthamiana* plants as described previously (Dalmay et al., 1993).

RNA Extraction and Analysis

Total RNA extraction from 100 mg of leaf tissue and RNA gel blot analysis of higher molecular weight RNAs were carried out as previously described (Dalmay et al., 1993).

RNA Gel Blot Analysis of 21–26 nt RNAs

Five micrograms of total RNA was separated in 8% polyacrylamide, 8.3 M urea, 1× TBE gels. The gel was soaked in 20× SSC solution for 15 min and then RNA was blotted onto Hybond-N membranes and fixed by baking in an oven at 80°C for 2 hr. Strand-specific RNA probes were generated by in vitro RNA transcription from the indicated cDNA clones in the presence of [α-^{32}P] UTP. Hybridization was performed in 50% formamide, 5× SSPE, 5× Denhardt's solution, 0.5% SDS with competitor DNA. After overnight incubation at 40°C, the filter was washed twice in 2× SSC, 0.1% SDS for 10 min at 40°C.

Plant Materials

Wild-type *N. benthamiana* plants grown in soil under normal growth conditions were used for virus infection and agroinfiltration. After infection or infiltration, plants were grown in a FITOTRON plant growth room (Versatile Enviromental Test Chambers [Sanyo, Tokyo Japan]) under a 14 hr light (50 $\mu E \cdot m^{-2} \cdot s^{-1}$) and 10 hr dark regime at 22°C.

RNA Silencing Assay by Agro-Infiltration

To detect silencing suppressor activity of wild-type and mutant p19 of CIRV, the *A. tumefaciens* infiltration method (Voinnet et al., 1998) was used. *N. benthamiana* plants were infiltrated with an overnight culture of *A. tumefaciens* (OD_{600} = 1) carrying a 35S-GFP construct. For coinfiltration, equal volumes of a 35S-GFP expressing *A. tumefaciens* culture and an *A. tumefaciens* culture (OD_{600} = 1) expressing wild-type or mutant CIRV p19 suppressors were mixed as described by Silhavy et al. (2002).

GFP Imaging

Visual detection of GFP fluorescence was performed using a 100 W handheld long-wave ultraviolet lamp (UV products, Upland, California, Black Ray model B 100AP). Plants were photographed with a Canon EOS D30 digital camera using a Wratten 8 filter.

Acknowledgments

We thank K. Weeks, P. Zamore, D. Shock, and M. Ghosh for helpful discussions on performing and analyzing electrophoretic mobility shift assays; L. Pedersen for protein expression and crystallization advice; J. Krahn for computer support and advice on crystallography; the staff at the SER-CAT beamline at the Advanced Photon Source for help with data collection; and our colleagues for critical comments on the manuscript. Use of the Advanced Photon Source was supported by the U.S. Department of Energy, Office of Science, Office of Basic Energy Sciences, under Contract No. W-31-109-Eng-38. This research was supported by grants from the Hungarian Ministry of Education (NKFP 4/023/2001) and "VIS" EU project (QLG2-CT-2002-01673) and the intramural program of the National Institute of Environmental Health Sciences.

Received: October 30, 2003
Revised: December 3, 2003
Accepted: December 3, 2003
Published Online: December 5, 2003

References

Abrahams, J.P., and Leslie, A.G.W. (1996). Methods used in the structure determination of bovine mitochondrial F_1 ATPase. Acta Crystallogr. D *52*, 30–42.

Ahlquist, P. (2002). RNA-dependent RNA polymerases, viruses, and RNA silencing. Science *296*, 1270–1273.

Altschul, S.F., Madden, T.L., Schäffer, A.A., Zhang, J., Zhang, Z., Miller, W., and Lipman, D.J. (1997). Gapped BLAST and PSI-BLAST: a new generation of protein database search programs. Nucleic Acids Res. *25*, 3389–3402.

Anandalakshmi, R., Pruss, G.J., Ge, X., Marathe, R., Mallory, A.C., Smith, T.H., and Vance, V.B. (1998). A viral suppressor of gene silencing in plants. Proc. Natl. Acad. Sci. USA *95*, 13079–13084.

Bartel, B., and Bartel, D.P. (2003). MicroRNAs: at the root of plant development? Plant Physiol. *132*, 709–717.

Baulcombe, D.C. (1999). Fast forward genetics based on virus-induced gene silencing. Curr. Opin. Plant Biol. *2*, 109–113.

Baulcombe, D. (2002a). RNA silencing. Curr. Biol. *12*, R82–R84.

Baulcombe, D. (2002b). Viral suppression of systemic silencing. Trends Microbiol. *10*, 306–308.

Bernstein, E., Caudy, A.A., Hammond, S.M., and Hannon, G.J. (2001). Role for a bidentate ribonuclease in the initiation step of RNA interference. Nature *409*, 363–366.

Brigneti, G., Voinnet, O., Li, W.-X., Ji, L.-H., Ding, S.-W., and Baulcombe, D.C. (1998). Viral pathogenicity determinants are suppressors of transgene silencing in *Nicotiana benthamiana*. EMBO J. *17*, 6739–6746.

Brünger, A.T. (1992). Free R value: a novel statistical quantity for assessing the accuracy of crystal structures. Nature *355*, 472–475.

Brünger, A.T., Adams, P.D., Clore, G.M., DeLano, W.L., Gros, P., Grosse-Kunstleve, R.W., Jiang, J.-S., Kuszewski, J., Nilges, M., Pannu, N.S., et al. (1998). Crystallography & NMR system: A new software suite for macromolecular structure determination. Acta Crystallogr. D *54*, 905–921.

Burgyán, J., Rubino, L., and Russo, M. (1996). The 5′-terminal region of a tombusvirus genome determines the origin of multivesicular bodies. J. Gen. Virol. *77*, 1967–1974.

Chu, M., Desvoyes, B., Turina, M., Noad, R., and Scholthof, H.B. (2000). Genetic dissection of tomato bushy stunt virus p19-protein-mediated host-dependent symptom induction and systemic invasion. Virology *266*, 79–87.

Cogoni, C., and Macino, G. (2000). Post-transcriptional gene silencing across kingdoms. Curr. Opin. Genet. Dev. *10*, 638–643.

Collaborative Computational Project, Number 4. (1994). The CCP4 Suite: Programs for Protein Crystallography. Acta Crystallogr. D *50*, 760–763.

Dalmay, T., Rubino, L., Burgyán, J., Kollar, A., and Russo, M. (1993). Functional analysis of cymbidium ringspot virus genome. Virology *194*, 697–704.

de la Fortelle, E., and Bricogne, G. (1997). Maximum-likelihood heavy-atom parameter refinement for multiple isomorphous replacement and multiwavelength anomalous diffraction methods. Methods Enzymol. *276*, 472–494.

DeLano, W.L. (2002). The PyMOL User's Manual (San Carlos, CA: DeLano Scientific).

Elbashir, S.M., Harborth, J., Lendeckel, W., Yalcin, A., Weber, K., and Tuschl, T. (2001a). Duplexes of 21-nucleotide RNAs mediate RNA interference in cultured mammalian cells. Nature *411*, 494–498.

Elbashir, S.M., Lendeckel, W., and Tuschl, T. (2001b). RNA interference is mediated by 21- and 22-nucleotide RNAs. Genes Dev. *15*, 188–200.

Elbashir, S.M., Martinez, J., Patkaniowska, A., Lendeckel, W., and Tuschl, T. (2001c). Functional anatomy of siRNAs for mediating efficient RNAi in *Drosophila melanogaster* embryo lysate. EMBO J. *20*, 6877–6888.

Hamilton, A., Voinnet, O., Chappell, L., and Baulcombe, D. (2002). Two classes of short interfering RNA in RNA silencing. EMBO J. *21*, 4671–4679.

Hamilton, A.J., and Baulcombe, D.C. (1999). A species of small antisense RNA in posttranscriptional gene silencing in plants. Science *286*, 950–952.

Hammond, S.M., Boettcher, S., Caudy, A.A., Kobayashi, R., and Hannon, G.J. (2001). Argonaute2, a link between genetic and biochemical analyses of RNAi. Science *293*, 1146–1150.

Hannon, G.J. (2002). RNA interference. Nature *418*, 244–251.

Holm, L., and Sander, C. (1993). Protein structure comparison by alignment of distance matrices. J. Mol. Biol. *233*, 123–138.

Hull, R. (2002). Matthews' Plant Virology, Fourth edn (San Diego, CA: Academic Press).

Johansen, L.K., and Carrington, J.C. (2001). Silencing on the spot. Induction and suppression of RNA silencing in the *Agrobacterium*-mediated transient expression system. Plant Physiol. *126*, 930–938.

Jones, T.A., Zou, J.-Y., Cowan, S.W., and Kjeldgaard (1991). Improved methods for building protein models in electron density maps and the location of errors in these models. Acta Crystallogr. A *47*, 110–119.

Jung, J., and Lee, B. (2001). Circularly permuted proteins in the protein structure database. Protein Sci. *10*, 1881–1886.

Kasschau, K.D., and Carrington, J.C. (1998). A counterdefensive strategy of plant viruses: Suppression of posttranscriptional gene silencing. Cell *95*, 461–470.

Ketting, R.F., Fischer, S.E.J., Bernstein, E., Sijen, T., Hannon, G.J., and Plasterk, R.H.A. (2001). Dicer functions in RNA interference and in synthesis of small RNA involved in developmental timing in *C. elegans*. Genes Dev. *15*, 2654–2659.

Li, W.X., and Ding, S.W. (2001). Viral suppressors of RNA silencing. Curr. Opin. Biotechnol. *12*, 150–154.

Li, H., Li, W.X., and Ding, S.W. (2002). Induction and suppression of RNA silencing by an animal virus. Science *296*, 1319–1321.

Lin, S.-Y., and Riggs, A.D. (1972). *lac* repressor binding to non-operator DNA: detailed studies and a comparison of equilibrium and rate competition methods. J. Mol. Biol. *72*, 671–690.

Lovell, S.C., Davis, I.W., Arendall, W.B., III, de Bakker, P.I., Word, J.M., Prisant, M.G., Richardson, J.S., and Richardson, D.C. (2003). Structure validation by Cα geometry: ϕ,ψ and Cβ deviation. Proteins *50*, 437–450.

Luscombe, N.M., Laskowski, R.A., and Thornton, J.M. (1997). NUCPLOT: A program to generate schematic diagrams of protein-nucleic acid interactions. Nucleic Acids Res. *25*, 4940–4945.

Mallory, A.C., Reinhart, B.J., Bartel, D., Vance, V.B., and Bowman, L.H. (2002). A viral suppressor of RNA silencing differentially regulates the accumulation of short interfering RNAs and micro-RNAs in tobacco. Proc. Natl. Acad. Sci. USA *99*, 15228–15233.

Martinez, J., Patkaniowska, A., Urlaub, H., Luhrmann, R., and Tuschl, T. (2002). Single-stranded antisense siRNAs guide target RNA cleavage in RNAi. Cell *110*, 563–574.

Nicholls, A., Sharp, K.A., and Honig, B. (1991). Protein folding and association: Insights from the interfacial and thermodynamic properties of hydrocarbons. Proteins *11*, 281–296.

Nikulin, A., Eliseikina, I., Tishchenko, S., Nevskaya, N., Davydova, N., Platonova, O., Piendl, W., Selmer, M., Liljas, A., Drygin, D., et al. (2003). Structure of the L1 protuberance in the ribosome. Nat. Struct. Biol. *10*, 104–108.

Nykanen, A., Haley, B., and Zamore, P.D. (2001). ATP requirements and small interfering RNA structure in the RNA interference pathway. Cell *107*, 309–321.

Otwinowski, Z., and Minor, W. (1997). Processing of x-ray diffraction data collected in oscillation mode. Methods Enzymol. *276*, 307–326.

Papp, I., Mette, M.F., Aufsatz, W., Daxinger, L., Schauer, S.E., Ray, A., van der Winden, J., Matzke, M., and Matzke, A.J.M. (2003). Evidence for nuclear processing of plant micro RNA and short interfering RNA precursors. Plant Physiol. *132*, 1382–1390.

Park, W., Li, J., Song, R., Messing, J., and Chen, X. (2002). CARPEL FACTORY, a Dicer homolog, and HEN1, a novel protein, act in microRNA metabolism in *Arabidopsis thaliana*. Curr. Biol. *12*, 1484–1495.

Provost, P., Silverstein, R.A., Dishart, D., Walfridsson, J., Djupedal, I., Kniola, B., Wright, A., Samuelsson, B., Rådmark, O., and Ekwall, K. (2002). Dicer is required for chromosome segregation and gene silencing in fission yeast cells. Proc. Natl. Acad. Sci. USA *99*, 16648–16653.

Qiu, W., Park, J.-W., and Scholthof, H.B. (2002). Tombusvirus P19-mediated suppression of virus-induced gene silencing is controlled by genetic and dosage features that influence pathogenicity. Mol. Plant Microbe Interact. *15*, 269–280.

Qu, F., and Morris, T.J. (2002). Efficient infection of *Nicotiana benthamiana* by Tomato bushy stunt virus is facilitated by the coat protein and maintained by p19 through suppression of gene silencing. Mol. Plant Microbe Interact. *15*, 193–202.

Scholthof, H.B., Scholthof, K.-B.G., and Jackson, A.O. (1995). Identification of tomato bushy stunt virus host-specific symptom determinants by expression of individual genes from a potato virus X vector. Plant Cell *7*, 1157–1172.

Schwarz, D.S., Hutvágner, G., Du, T., Xu, Z., Aronin, N., and Zamore, P.D. (2003). Asymmetry in the assembly of the RNAi enzyme complex. Cell *115*, 199–208.

Silhavy, D., Molnár, A., Lucioli, A., Szittya, G., Hornyik, C., Tavazza, M., and Burgyán, J. (2002). A viral protein suppresses RNA silencing and binds silencing-generated, 21- to 25-nucleotide double-stranded RNAs. EMBO J. *21*, 3070–3080.

Szittya, G., Molnár, A., Silhavy, D., Hornyik, C., and Burgyán, J. (2002). Short defective interfering RNAs of tombusviruses are not targeted but trigger post-transcriptional gene silencing against their helper virus. Plant Cell *14*, 359–372.

Szittya, G., Silhavy, D., Molnár, A., Havelda, Z., Lovas, A., Lakatos, L., Banfalvi, Z., and Burgyán, J. (2003). Low temperature inhibits RNA silencing-mediated defence by the control of siRNA generation. EMBO J. *22*, 633–640.

Tang, G., Reinhart, B.J., Bartel, D.P., and Zamore, P.D. (2003). A biochemical framework for RNA silencing in plants. Genes Dev. *17*, 49–63.

Voinnet, O. (2001). RNA silencing as a plant immune system against viruses. Trends Genet. *17*, 449–459.

Voinnet, O. (2002). RNA silencing: small RNAs as ubiquitous regulators of gene expression. Curr. Opin. Plant Biol. *5*, 444–451.

Voinnet, O., Vain, P., Angell, S., and Baulcombe, D.C. (1998). Systemic spread of sequence-specific transgene RNA degradation in plants is initiated by localized introduction of ectopic promoterless DNA. Cell *95*, 177–187.

Voinnet, O., Pinto, Y.M., and Baulcombe, D.C. (1999). Suppression of gene silencing: A general strategy used by diverse DNA and RNA viruses of plants. Proc. Natl. Acad. Sci. USA *96*, 14147–14152.

Volpe, T.A., Kidner, C., Hall, I.M., Teng, G., Grewal, S.I.S., and Martienssen, R.A. (2002). Regulation of heterochromatic silencing and histone H3 lysine-9 methylation by RNAi. Science *297*, 1833–1837.

Wang, B.C. (1985). Resolution of phase ambiguity in macromolecular crystallography. Methods Enzymol. *115*, 90–112.

Waterhouse, P.M., Smith, N.A., and Wang, M.-B. (1999). Virus resistance and gene silencing: Killing the messenger. Trends Plant Sci. *4*, 452–457.

Weeks, K.M., and Crothers, D.M. (1992). RNA binding assays for Tat-derived peptides: Implications for specificity. Biochemistry *31*, 10281–10287.

Yusupov, M.M., Yusupova, G.Z., Baucom, A., Lieberman, K., Earnest, T.N., Cate, J.H.D., and Noller, H.F. (2001). Crystal structure of the ribosome at 5.5 Å resolution. Science *292*, 883–896.

Zamore, P.D., Tuschl, T., Sharp, P.A., and Bartel, D.P. (2000). RNAi: double-stranded RNA directs the ATP-dependent cleavage of mRNA at 21 to 23 nucleotide intervals. Cell *101*, 25–33.

Zilberman, D., Cao, X., and Jacobsen, S.E. (2003). ARGONAUTE4 control of locus-specific siRNA accumulation and DNA and histone methylation. Science *299*, 716–719.

Accession Numbers

The coordinates and structure factors for the structure of CIRVp19 in complex with siRNA have been deposited with the Protein Data Bank ID code 1RPU.